Mapping the limits of equilibrium in sheared granular liquid crystals

Jacopo Bilotto [1,*] Martin Trulsson [2] and Jean-François Molinari [1]
[1]*Institute of Civil Engineering, Institute of Materials Science and Engineering, École Polytechnique Fédérale de Lausanne (EPFL), CH-1015 Lausanne, Switzerland*
[2]*Computational Chemistry, Lund University, SE-221 00 Lund, Sweden*

(Received 26 March 2026; accepted 14 October 2026; published 10 November 2026)

While elongated particles in viscous fluids follow Jeffery orbits, their dynamics in dense granular flows remain unresolved. We demonstrate that sheared, low-friction granular rods do not follow these orbits, but instead reach a quasiequilibrium state quantitatively described by classical liquid crystal theory, with collisions providing effective thermal noise. This quasiequilibrium analogy breaks down at two limits: low aspect ratios, where the theory incorrectly predicts isotropy, and high interparticle friction, which drives a transition from steric screening to frictional gearing. We map this far-from-equilibrium breakdown using a phenomenological effective Ericksen number, establishing the limits of thermal thermodynamic analogies in driven athermal matter.

DOI: 10.1103/cjdt-6d9p

I. INTRODUCTION

Granular materials, though athermal and dissipative, can surprisingly arrange into ordered, equilibriumlike configurations when driven [1]. Elongated grains, for instance, exhibit isotropic-nematic transitions driven purely by geometric steric exclusion [2–4] and align in shear flows [5–11], even at modest shape anisotropies [12]. This behavior strongly resembles the isotropic-to-nematic transition of thermal liquid crystals, which is well described by equilibrium Onsager statistical mechanics in dilute systems [13] and by Parsons's [14] and Lee' [15] correction for high density. The nonequilibrium driving is also effectively captured in the Doi-Edwards-Kuzuu (DEK) framework [16–18], which quantitatively describes these thermal systems under flow. Although attempts have been made to model the ordering of granular monolayers [19], a corresponding statistical tool is currently lacking for athermal systems. Treating collisions as an effective source of thermal noise [20] has emerged as a promising pathway to formulate an out-of-equilibrium theory. Using classical equilibrium theory, we show that this approach accurately predicts the orientation distribution of elongated grains, provided the grains are sufficiently elongated and with low friction. However, the analogy breaks down when the nonequilibrium rotational driving overwhelms the steric caging. In our specific system, this divergence manifests both at low anisotropies, where steric caging is inherently weak, and at high interparticle friction. At higher elongations, crossing this threshold triggers a transition from a quasiequilibrium steric "screening" state to a far-from-equilibrium frictional "gearing" state.

II. METHODS

To investigate the alignment of athermal granular systems under shear, we employ a discrete element method with soft-core Hertz-Mindlin frictional interactions, a Coulomb friction coefficient μ_p, and a normal restitution coefficient of 0.1. All systems consist of $N = 2000$ spheroids with a 20% degree of polydispersity [21], and are sheared through Lees-Edwards boundary conditions [22] at constant normal stress σ_{yy}, imposed along the gradient direction, maintaining an inertial number $I = \dot{\gamma} d\sqrt{\rho/\sigma_{yy}} \approx 0.1$, where $\dot{\gamma}$ is the shear rate, d the particle equivalent sphere diameter, and ρ its density. We have checked that an almost linear velocity profile is achieved for all simulations. The contact stiffness number $\kappa = (E/\sigma_{yy})^{2/3} > 2 \times 10^3$, with E the grains' Young's modulus, is set sufficiently high to ensure that the overlap between grains is small. A snapshot of the simulation setup is shown in Fig. 1(a). Orientation statistics are calculated by averaging over all particles in steady state, (see A in the Supplemental Material [23], extracted after an accumulated strain of $\gamma = 20$, and time-averaged over an additional ten strain units (1000 snapshots) yielding 2×10^6 distinct particle configurations per run. Further simulation details are provided in Ref. [11] and robustness checks are provided in B in the Supplemental Material [23]. While our primary parametric study employs spheroids (as depicted in Fig. 1), we performed an additional, targeted set of simulations using rodlike superellipsoids (detailed in C in the Supplemental Material [23]) to accurately validate our model against the cylindrical grains used in experimental data [5,6,24,25]. These validation runs followed the same protocol as the spheroid simulations. Experimental comparisons are made with data from these references, which were obtained with x-ray computed tomography scans

*Contact author: jacopo.bilotto@epfl.ch

Published by the American Physical Society under the terms of the Creative Commons Attribution 4.0 International license. Further distribution of this work must maintain attribution to the author(s) and the published article's title, journal citation, and DOI.

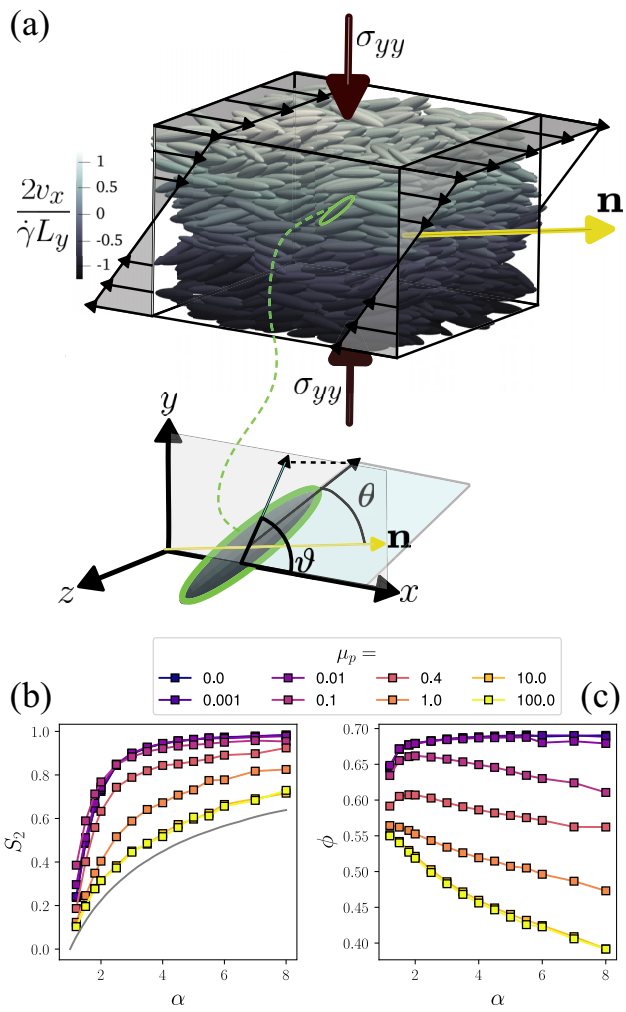


FIG. 1. (a) Shear cell for $\alpha = 5.0$, $\mu_p = 0.4$, with particles colored by their normalized flow velocity, v_f, with respect to the uniform gradient $\dot{\gamma}L_y/2$, L_y being the average box length in the gradient direction. A constant normal stress, σ_{yy}, is applied along the gradient direction. The yellow arrow indicates the macroscopic director $\mathbf{n}$. For a representative particle (highlighted in green), the in-plane angle ϑ with respect to the flow and the polar angle θ with respect to the director are explicitly shown. (b) Nematic order parameter S_2 and (c) packing fraction ϕ as a function of aspect ratio α. The plots show that increasing interparticle friction μ_p (from dark blue to yellow) reduces nematic ordering (lowering S_2) and induces dilatancy (lowering ϕ). The gray line marks the theoretical prediction for Jeffery orbits, without noise or steric interaction, starting from an isotropic distribution, as done in Ref. [20]. All the data lie above this prediction, confirming that Jeffery orbits are not sufficient to describe the dense granular flows. The color scheme for μ_p is used in subsequent figures.

in split-bottom shear cell measurements and averaged over long strains in the shearing zone.

III. MATHEMATICAL FRAMEWORK

With this physical system established, we look for the appropriate mathematical framework to describe the steady-state orientational statistics. We test whether the continuum framework originally developed for thermal nematic suspensions can be adapted for driven athermal grains.

Consider an axisymmetric particle with aspect ratio $\alpha > 1$ in a simple shear flow at high packing fraction. To model how these particles collectively align, we track their orientation distribution $f(\mathbf{u})$, where $\mathbf{u}$ is the unit vector defining the orientation of the particle's major axis. The preferred macroscopic orientation is the director $\mathbf{n}$ (principal eigenvector of $\langle \mathbf{u} \otimes \mathbf{u} \rangle$), lying in the flow-gradient plane at an angle η to the flow. Particle orientations are described by the polar angle from the director, $\theta = \arccos(\mathbf{u} \cdot \mathbf{n})$, and the in-plane alignment angle, $\vartheta = \arctan(u_y/u_x)$, see inset of Fig. 1(a). Following DEK theory [17,26], the evolution of this distribution is governed by a Smoluchowski-type equation, which balances the rotation driven by the macroscopic flow against the effective diffusion caused by interparticle collisions. In athermal systems under simple shear flow, the rotational diffusion D_r scales linearly with shear rate $\dot{\gamma}$ (see D in the Supplemental Material [23]), such that $D_r = \tilde{D}_r(f(\mathbf{u}))\dot{\gamma}$, where the mobility $\tilde{D}_r(f)$ is, in our case, derived from extended tube models [27]. In these models, the dense surrounding neighbors act as a tight physical cage, the "tube," severely restricting the particle's ability to rotate. Additionally, solid contacts [28] alter the deterministic torque relative to the dilute Jeffery orbit [29]. While closed-form microscopic expression for the drift remains an open challenge [30], our general framework might in principle apply to different classes of interactions, of different physical origins. We define this effective driving flux as $\mathcal{J}(\mathbf{u})$. Eliminating time in favor of accumulated strain γ [24], the evolution equation is

$$\frac{\partial f}{\partial \gamma} + \nabla_{\mathbf{u}} \cdot [\tilde{\mathcal{J}} f] = \tilde{D}_r(f) \nabla_{\mathbf{u}} \cdot [\nabla_{\mathbf{u}} f + f \nabla_{\mathbf{u}} \mathcal{U}_{\text{ex}}], \quad (1)$$

where $\nabla_{\mathbf{u}} = (\mathbf{I} - \mathbf{u} \otimes \mathbf{u}) \cdot \frac{\partial}{\partial \mathbf{u}}$ is the gradient operator on the unit sphere, $\mathbf{I}$ being the identity tensor, $\tilde{\mathcal{J}} = \mathcal{J}/\dot{\gamma}$ is the normalized driving, and $\mathcal{U}_{\text{ex}}$ is the mean-field steric potential [13,14]. If the driving flux balances the restoring diffusion (in the weak shearing limit [31]), the steady state ($\partial_\gamma f = 0$) recovers the extended Maier-Saupe equilibrium distribution [32]:

$$f_{\text{eq}}(\theta) = \frac{1}{Z} \exp\left(U_2 S_2 P_2(\cos\theta) + U_4 S_4 P_4(\cos\theta)\right), \quad (2)$$

where Z is a normalization constant, θ is the angle with the director of the distribution, $S_{2,4} = \langle P_{2,4}(\cos\theta) \rangle$ are the second and fourth nematic order parameters, respectively, and $P_{2,4}$ are the second- and fourth-order Legendre polynomials. $U_{2,4}$ are the shape-dependent steric strengths. Here, the operator $\langle \cdots \rangle = \int \cdots f(\mathbf{u}) d\mathbf{u}$ denotes the ensemble average. To generate our theoretical predictions, these strengths are computed explicitly from the particles' excluded volume using the Parsons-Lee approach and the Berne-Pechukas [33] approximation (see E in the Supplemental Material [23] for the full derivation [34,35] and F in the Supplemental Material [23] for finite grain stiffness effects [36]). Physically, this distribution describes a steady state where steric exclusion forces the particles to preferentially align along a common axis, with S_2 and S_4 quantifying the sharpness of this alignment. Crucially, while an equivalent thermal system would crystallize at the high volume fractions recorded here, the imposed

shear continuously disrupts translational order. This forced shear melting sustains a flowing [37], supercooled nematic state. Consequently, the macroscopic driving not only forces nematic alignment at low aspect ratios (where equilibrium predicts an isotropic phase), but also allows highly elongated grains to achieve stronger nematic ordering at high densities without freezing into a smectic or crystalline solid.

IV. RESULTS

With this theoretical baseline established, we can evaluate how well it captures the behavior of our highly dissipative, driven system. Figure 1(b) shows the measured nematic ordering as a function of elongation and friction: as previously found [9–11], S_2 rises with α, but friction generally reduces ordering. This disordering correlates with a drop in average volume fraction, ϕ, due to frictional dilatancy [Fig. 1(c)]. Crucially, the data lie above the prediction for isolated Jeffery orbits (gray line) [20], indicating that steric interactions are essential to maintain order in dense flows. Additionally, the data for $\mu = 10$ and $\mu_p = 100$ overlap. While these extreme values exceed standard tribological measurements, they serve to establish the theoretical infinite-friction limit, where virtually all contacts are sticking.

For both simulations and experiments [5,24] (see A in the Supplemental Material [23]), the particles reach a steady average angle of alignment toward the extension direction, with no tumbling or wagging of the director. Nevertheless, a stable director simply indicates a time-invariant orientational distribution; individual particles may still undergo continuous rotation [20], yielding a nonzero mean angular velocity. Equation (1) with $\tilde{\mathcal{J}}$ corresponding to the Jeffery operator would erroneously predict tumbling at low shear rates or alignment toward the compression direction at high shear rates [26]. This motivates us to find an empirical expression for the driving, by directly measuring it from our simulations, quantified by the mean angular velocity $\langle\omega_z\rangle$ in the vorticity direction. We observe that the suppression of order coincides with a transition in rotational dynamics. By measuring the average normalized angular velocity $\tilde{\omega} = -2\langle\omega_z\rangle/\dot{\gamma}$, we identify two distinct regimes [Fig. 2(a)]. In the frictionless limit ($\mu_p \to 0$), $\tilde{\omega}$ vanishes at high elongation. This is the "steric screening" state: collective nematic alignment generates a steric potential that effectively cancels the shear torque, preventing rotation [Fig. 2(b), dark curves showing the conditionally averaged angular velocity $\langle\omega_z\rangle_\vartheta$ for particles oriented at angle ϑ]. Conversely, at high friction ($\mu_p \geqslant 1.0$), $\tilde{\omega}$ becomes large, exceeding even the viscous Jeffery prediction [29,38]. Although this resembles the injection of noise in viscous systems [20], interparticle friction increases the actual driving torque alongside the noise. Therefore, the system never simply reduces to the infinite-noise fluid limit, i.e., uniform rotation with the background fluid. This is the "frictional gearing" state: sliding is suppressed and nonhydrodynamic contacts force particles to tumble (yellow curves). As a simple explanation, consider the limit of infinitely slender particles. If they are perfectly aligned with the flow, frictional particles cannot slide, resulting in a finite torque even for thin rods perfectly aligned with the flow, which explains why they can roll more than the Jeffery prediction. This transition is well described

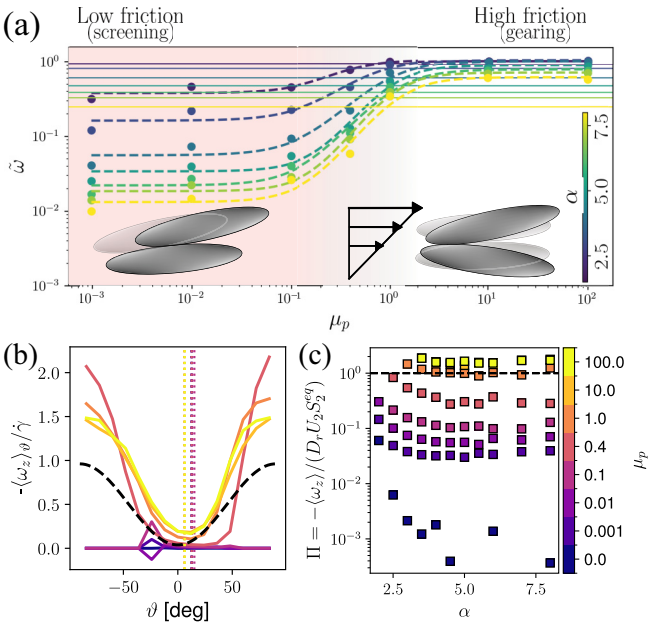


FIG. 2. Quantifying the "screening-to-gearing" transition. (a) Normalized average angular velocity $\tilde{\omega}$ extracted from simulations across varying friction coefficients (markers). Colors denote the particle aspect ratio α. Solid lines represent the theoretical Jeffery prediction for an isolated particle in a viscous fluid, which fails to capture the dense granular dynamics. Instead, the data are well described by a two-state phenomenological model (dashed lines) capturing the transition between a low-friction "screening" state and a high-friction "gearing" state. In the gearing state, grains rotate faster than the isolated particle prediction, whereas in the screening state, their rotation is severely hindered. (b) Normalized conditional angular velocity $-\langle\omega_z\rangle_\vartheta/\dot{\gamma}$ vs the angle with respect to the flow direction, ϑ, for $\alpha = 5.0$. The dashed black line represents the theoretical prediction for Jeffery orbits, while the vertical dotted lines indicate the measured director angle (η) in the flow-gradient plane. In the low-friction "screening" regime (dark curves, $\mu_p \leqslant 0.01$), $\tilde{\omega} \approx 0$ as steric forces (director at η, dotted lines) cancel the shear torque (Jeffery orbit, black dashed line), meaning the aligned grains effectively lock into place and slide past one another without spinning. In the high-friction "gearing" regime (yellow curves, $\mu_p \geqslant 1.0$), $\tilde{\omega}$ is large, showing strong rotational driving. (c) The effective Ericksen number Π shows the consequence. The system is in the quasiequilibrium limit ($\Pi \ll 1$) for low friction. As μ_p increases, Π grows by orders of magnitude, crossing the $\Pi = 1$ threshold (dashed black line) and signaling a transition to a far-from-equilibrium, drive-dominated state.

by a phenomenological sigmoid function [dashed lines; see Eq. (S20) in the Supplemental Material [23]], which models the crossover from sliding to rolling contacts [10,11,39], using physically consistent fit parameters.

To quantify the balance between nonequilibrium driving and equilibrium-restoring effects, we derive a diagnostic dimensionless parameter Π. This parameter, an effective Ericksen number [40], directly compares the characteristic rates of the competing fluxes in Eq. 1. The nonequilibrium driving flux, which forces tumbling, is set by the phenomenologically determined rotational driving, $\mathcal{J} \sim \langle\omega_z\rangle$. The quasiequilibrium-restoring flux arises from the system'

attempt to return to the nematic state f_{eq}, and scales as the rotational diffusion D_r multiplied by the characteristic theoretical gradient of the steric potential, $|\nabla_{\mathbf{u}}\mathcal{U}_{\text{ex}}| \sim U_2 S_2^{\text{eq}}$, where S_2^{eq} is the nematic order parameter from equilibrium theory and we neglected the smaller contribution of the P_4 term. The ratio of these two competing rates, which is the ratio of the two governing dimensionless numbers, defines Π:

$$\Pi = -\frac{\langle \omega_z \rangle}{D_r U_2 S_2^{\text{eq}}}. \tag{3}$$

This parameter maps the system's state: the quasiequilibrium "screening" regime corresponds to $\Pi \ll 1$, where restoring steric flux dominates, while the far-from-equilibrium "gearing" regime corresponds to $\Pi \gg 1$, where driving dominates. Figure 2(c) shows that $\Pi < 1$ for $\mu_p \leqslant 0.4$, and even in the infinite frictional limit, where virtually all the contacts are sticking, Π stays finite and order one. However, as shape anisotropy decreases, the system undergoes a transition yielding a close-to-isotropic state. In this regime, the system is inherently nonequilibrium: there is no preexisting order to screen the flow. The dynamics are no longer a balance of fluxes but are dictated solely by the driving strength, making the rotational Péclet number, $\text{Pe} = \langle \omega_z \rangle / D_r = \Pi\, U_2\, S_2$, the relevant control parameter. This is evidenced by the consistently nonzero values of the nematic parameter observed even at very small elongations [12,41].

The breakdown of the equilibrium analogy is visualized in the orientational distributions [Fig. 3(a)]. These distributions are measured around the director and limited to the polar angle, to focus on the breadth of the distribution (see H in the Supplemental Material [23] for flow-induced anisotropy). As expected, higher aspect ratios produce progressively sharper peaks. However, increasing friction ($\Pi > 1$) broadens the distributions, and the equilibrium Onsager-Parsons-Lee theory systematically fails, confirming the breakdown of the equilibrium analogy. The continuous lines present the prediction from the Parsons-Lee equilibrium theory [14,15] (see E in the Supplemental Material [23]). At high aspect ratio and low friction, the data and the theory show excellent overlap. However, these distributions reveal the two distinct failure modes of the equilibrium framework. First, at low α ($\alpha < 2.5$), the equilibrium theory predicts an isotropic state ($S_2^{\text{eq}} \approx 0$) due to negligible steric interactions, whereas the simulation data (dots) reveal shear-induced nematic ordering driven by the nonequilibrium alignment term $\tilde{\mathcal{J}}$. Second, at high friction ($\mu_p = 10.0$) and high α, the theory predicts a much sharper peak than observed. Here, the nonequilibrium "frictional gearing" ($\Pi \gg 1$) actively disorders the system, broadening the distribution beyond the thermal prediction. This broadening is sensitive to the inertial number I, unlike the robust quasiequilibrium regime (see B in the Supplemental Material [23]).

To confirm the robustness of these findings across different particle shapes and beyond ideal simulations, we carried out additional simulations of superellipsoidal rodlike particles (see C in the Supplemental Material [23]) and compared our framework directly against experimental measurements of granular rods from Ref. [6]. As shown in Fig. 3(b), at moderate and high elongations, there is a great correspondence between the split-bottom shear cell experiments and our simple shear rod simulations. To directly compare the theory

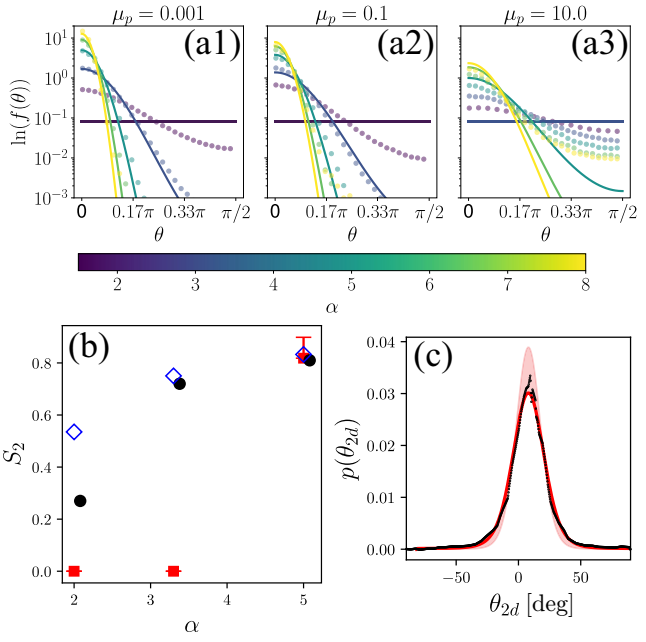


FIG. 3. (a1)–(a3) Log-scale orientational distributions $f(\theta)$ (markers) compared to the equilibrium Maier-Saupe theory [Eq. (2), solid lines]. The data reveal the breakdown of the equilibrium analogy as friction increases. (Left) In the low-friction, screening regime ($\mu_p = 0.001$), the theory accurately predicts the simulation data at high elongation, but fails at small α. (Middle) In the intermediate-friction case ($\mu_p = 0.1$), the simulated distributions become noticeably broader than predicted, though the theory still qualitatively captures the overall trends. (Right) In the high-friction, gearing regime ($\mu_p = 10.0$), the theory fails, underestimating the broadening of the distribution even at high α. Within each panel, colors represent aspect ratio α, with higher α (yellow) leading to stronger ordering (sharper peaks). (b) Nematic order parameter S_2 as a function of aspect ratio α, comparing experimental measurements [6] (black circles) with equilibrium theory predictions (red squares) and average for simple shear rod simulations with $\mu_p \in (0.1, 0.7)$ (blue hollow diamonds). Theoretical points are shifted slightly along the horizontal axis for visual clarity. At small elongations, the theory predicts an isotropic state ($S_2 \approx 0$) rather than the observed nematic distribution. Conversely, at high friction the order parameter is remarkably close to the one from equilibrium theory. At moderate and high elongations, there is a great correspondence between split-bottom shear cell experiments and simple shear simulations. Red error bars represent the upper theoretical bounds assuming a +10% uncertainty (underestimation) in the experimentally measured volume fraction. (c) Comparison of the experimental in-plane orientation distribution $p(\theta_{2d})$ for $\alpha = 5$ (black dotted line) [6] against a theoretical reconstruction (red solid line). The reconstruction represents a two-dimensional (2D) projection of the uniaxial three-dimensional (3D) distribution estimated from the measured nematic order parameter, shifted to align with the experimentally measured average in-plane angle. The red shaded region reflects a plausible +10% uncertainty in the experimentally measured volume fraction due to binarization.

with experimental distributions, we reconstruct the theoretical equilibrium 3D distribution, using only the experimentally measured volume fraction ϕ, and project it onto the 2D plane, which mathematically averages out the out-of-plane orienta-

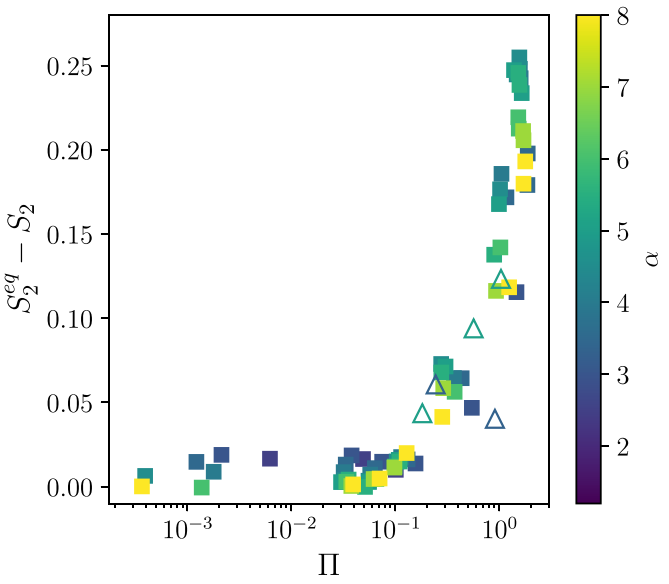


FIG. 4. The positive deviation between the measured nematic order parameter and the equilibrium prediction, $S_2^{\mathrm{eq}} - S_2$, plotted against the effective Ericksen number Π. Data points include both spheroid (squares) and superellipsoidal rod (hollow triangles) simulations for different aspect ratios. The collapse confirms that Π acts as a control parameter: for $\Pi \ll 1$ (steric screening), the system remains in a quasiequilibrium state with minimal deviation, while for $\Pi \gtrsim 1$ (frictional gearing), the system is driven far from equilibrium, leading to a systematic divergence from the theoretical prediction.

tions to mimic the view of the experimental camera:

$$p(\theta_{2d}) = \frac{1}{\pi |\cos\theta_{2d}|} \int_0^{\cos\theta_{2d}} \frac{t\, f_{\mathrm{eq}}(\arccos t)}{\sqrt{\cos^2\theta_{2d} - t^2}} dt, \qquad (4)$$

where $t = \cos\theta$. As shown in Fig. 3 (bottom panels), the reconstructed S_2 mirrors the trends observed in simulations: the theory captures the strong alignment at high α but fails to predict the shear-induced ordering at low α. Crucially, for $\alpha = 5.0$, the projected theoretical distribution shows excellent agreement with the experimental data, validating that the quasiequilibrium description holds for real dissipative granular media in the steric screening regime.

Finally, we utilize both the spheroid and rod simulation datasets to test our diagnostic metric Π. In Fig. 4, we show the deviation of the equilibrium nematic order parameter from the one measured in simulations $S_2^{\mathrm{eq}} - S_2$. We only show positive deviations since negative ones are associated with low α values $\alpha \leqslant 2.5$, where the equilibrium alignment is mainly dictated by the shear. The data show a nice collapse as a function of Π, for both rods and ellipsoids. At low Π, there is virtually no discrepancy, whereas as Π increases there is a clear correlation with the distance from equilibrium. This confirms that Π is the correct metric to gauge distance from equilibrium for those grains elongated enough so that their distribution would be nematic in a thermal system.

V. CONCLUSIONS AND OUTLOOK

In summary, we have shown that the orientational statistics of frictionless elongated granular particles under steady shear are quantitatively described by a mean-field Onsager-like theory, originally developed for thermal systems, when corrected via the Parsons-Lee scaling. This confirms the existence of a "quasiequilibrium" nematic state in a driven dissipative system, proving that simple noisy Jeffery orbits are insufficient to model the dynamics once steric interactions become significant. However, as interparticle friction is introduced, the system is driven far from equilibrium, and the equilibrium analogy systematically breaks. We show that this breakdown manifests as a transition from a "steric screening" state to a "frictional gearing" state, where contacts actively promote particle rotation. This transition is well captured by a simple phenomenological model, whose parameters show clear physical trends with particle shape. We quantify this with an effective Ericksen number, taken as the ratio of the driving over the restoring nematic torque, akin to active matter [42] that captures the distance from equilibrium for sufficiently elongated grains. By leaving the specific microscopic driving flux as an agnostic input, our architecture remains decoupled from purely granular contact mechanics. This allows the dimensionless breakdown diagnostic Π to serve as a general blueprint for other dense far-from-equilibrium anisotropic systems. The framework established here provides a new, parameter-free tool to map out nonequilibrium ordering transitions not only in advanced kinetic granular theories [43,44], but also in dense driven suspensions [45,46] and active matter [42], defining the boundary where equilibrium analogies fail.

ACKNOWLEDGMENTS

This project has received funding from the European Union's Horizon 2020 research and innovation program under the Marie Skłodowska-Curie Grant Agreement No. 945363. J.B. and J.-F.M. acknowledge financial support from Bühler AG. M.T. acknowledges funding from the Swedish Research Council under Grant No. 2021-04997. We also acknowledge helpful discussions with Tamás Börzsönyi and Pierpaolo Bilotto.

Conceptualization: J.B., M.T., and J.-F.M. Data curation: J.B. Formal analysis: J.B. and M.T. Funding acquisition: J.B., M.T., and J.-F.M. Investigation: J.B. Methodology: J.B. and M.T. Software: J.B. Supervision: M.T. and J.-F.M. Visualization: J.B. Writing—original draft: J.B. Writing—review & editing: M.T. and J.-F.M.

There are no conflicts to declare.

DATA AVAILABILITY

Data to support these findings are available on Zenodo [47]. Codes to run the simulations and the analysis are available on GitHub [48].

[1] P. M. Reis, R. A. Ingale, and M. D. Shattuck, Crystallization of a quasi-two-dimensional granular fluid, Phys. Rev. Lett. **96**, 258001 (2006).

[2] J. Galanis, D. Harries, D. L. Sackett, W. Losert, and R. Nossal, Spontaneous patterning of confined granular rods, Phys. Rev. Lett. **96**, 028002 (2006).

[3] J. Galanis, R. Nossal, W. Losert, and D. Harries, Nematic order in small systems: Measuring the elastic and wall-anchoring constants in vibrofluidized granular rods, Phys. Rev. Lett. **105**, 168001 (2010).

[4] T. Börzsönyi and R. Stannarius, Granular materials composed of shape-anisotropic grains, Soft Matter **9**, 7401 (2013).

[5] T. Börzsönyi, B. Szabó, G. Törös, S. Wegner, J. Török, E. Somfai, T. Bien, and R. Stannarius, Orientational order and alignment of elongated particles induced by shear, Phys. Rev. Lett. **108**, 228302 (2012).

[6] S. Wegner, T. Börzsönyi, T. Bien, G. Rose, and R. Stannarius, Alignment and dynamics of elongated cylinders under shear, Soft Matter **8**, 10950 (2012).

[7] D. Berzi, N. Thai-Quang, Y. Guo, and J. Curtis, Stresses and orientational order in shearing flows of granular liquid crystals, Phys. Rev. E **93**, 040901 (2016).

[8] D. Berzi, N. Thai-Quang, Y. Guo, and J. Curtis, Collisional dissipation rate in shearing flows of granular liquid crystals, Phys. Rev. E **95**, 050901 (2017).

[9] M. Trulsson, Rheology and shear jamming of frictional ellipses, J. Fluid Mech. **849**, 718 (2018).

[10] D. B. Nagy, P. Claudin, T. Börzsönyi, and E. Somfai, Flow and rheology of frictional elongated grains, New J. Phys. **22**, 073008 (2020).

[11] J. Bilotto, M. Trulsson, and J.-F. Molinari, Shear flow of frictional spheroids: Comparison between elongated and flattened particles, Phys. Rev. E **112**, 045432 (2025).

[12] T. Marschall, Y.-E. Keta, P. Olsson, and S. Teitel, Orientational ordering in athermally sheared, aspherical, frictionless particles, Phys. Rev. Lett. **122**, 188002 (2019).

[13] L. Onsager, The effects of shape on the interaction of colloidal particles, Ann. N. Y. Acad. Sci. **51**, 627 (1949).

[14] J. D. Parsons, Nematic ordering in a system of rods, Phys. Rev. A **19**, 1225 (1979).

[15] S.-D. Lee, A numerical investigation of nematic ordering based on a simple hard-rod model, J. Chem. Phys. **87**, 4972 (1987).

[16] M. Doi and S. F. Edwards, Dynamics of rod-like macromolecules in concentrated solution. Part 1, J. Chem. Soc. Faraday Trans. 2 **74**, 560 (1978).

[17] M. Doi, Molecular dynamics and rheological properties of concentrated solutions of rodlike polymers in isotropic and liquid crystalline phases, J. Polym. Sci.: Polym. Phys. Ed. **19**, 229 (1981).

[18] N. Kuzuu and M. Doi, Constitutive equation for nematic liquid crystals under weak velocity gradient derived from a molecular kinetic equation. II. Leslie coefficients for rodlike polymers, J. Phys. Soc. Jpn. **53**, 1031 (1984).

[19] T. Müller, D. de las Heras, I. Rehberg, and K. Huang, Ordering in granular-rod monolayers driven far from thermodynamic equilibrium, Phys. Rev. E **91**, 062207 (2015).

[20] J. Talbot, C. Antoine, P. Claudin, E. Somfai, and T. Börzsönyi, Exploring noisy Jeffery orbits: A combined Fokker-Planck and Langevin analysis in two and three dimensions, Phys. Rev. E **110**, 044143 (2024).

[21] Simulations with no polydispersity showed little difference in the results.

[22] A. W. Lees and S. F. Edwards, The computer study of transport processes under extreme conditions, J. Phys. C **5**, 1921 (1972).

[23] See Supplemental Material at https://link.aps.org/supplemental/10.1103/cjdt-6d9p for extended methodological details and supporting data analysis. It includes validations of the nonequilibrium steady state and rotational diffusion scaling, detailed excluded volume computations, and values of the phenomenological model parameters. Additionally, it presents measurements of flow-induced biaxiality, robustness checks across different simulation ensembles and inertial numbers, extended validation using rodlike particles, and a global accuracy map of the equilibrium theory.

[24] T. Börzsönyi, B. Szabó, S. Wegner, K. Harth, J. Török, E. Somfai, T. Bien, and R. Stannarius, Shear-induced alignment and dynamics of elongated granular particles, Phys. Rev. E **86**, 051304 (2012).

[25] S. Wegner, R. Stannarius, A. Boese, G. Rose, B. Szabó, E. Somfai, and T. Börzsönyi, Effects of grain shape on packing and dilatancy of sheared granular materials, Soft Matter **10**, 5157 (2014).

[26] R. G. Larson, Arrested tumbling in shearing flows of liquid-crystal polymers, Macromolecules **23**, 3983 (1990).

[27] S. Chen, W. Yan, and T. Gao, Scaling law of Brownian rotation in dense hard-rod suspensions, Phys. Rev. E **102**, 012608 (2020).

[28] A. Pol, R. Artoni, and P. Richard, Collective alignment controls rotation frustration in granular flows of elongated particles, Phys. Rev. Fluids **11**, 064302 (2026).

[29] G. B. Jeffery, The motion of ellipsoidal particles immersed in a viscous fluid, Proc. R. Soc. A **102**, 161 (1922).

[30] G. Quiñones and P. D. Olmsted, A Smoluchowski equation for a sheared suspension of frictionally interacting rods, J. Rheol. **70**, 1161 (2026).

[31] G. Marrucci and P. L. Maffettone, A description of the liquid-crystalline phase of rodlike polymers at high shear rates, Macromolecules **22**, 4076 (1989).

[32] W. Maier and A. Saupe, Eine einfache molekular-statistische Theorie der nematischen Kristallinflüssigen Phase. Teil II, Z. Naturforsch. A **15**, 287 (1960).

[33] B. J. Berne and P. Pechukas, Gaussian model potentials for molecular interactions, J. Chem. Phys. **56**, 4213 (1972).

[34] M. Piastra and E. G. Virga, Explicit excluded volume of cylindrically symmetric convex bodies, Phys. Rev. E **91**, 062503 (2015).

[35] B. C. Vega, Virial coefficients and equation of state of hard ellipsoids, Mol. Phys. **92**, 651 (1997).

[36] J. A. Barker and D. Henderson, Perturbation theory and equation of state for fluids: The square-well potential, J. Chem. Phys. **47**, 2856 (1967).

[37] Z. Zeng, J. Xu, H. Li, S. Zhang, H. Yuan, C. Zhou, X. Dai, H. Lu, X. Wang, J. Zhao, Y. Jiang, Z. Ge, G. Huang, C. Xia, J. Sun, Y. Xi, and Y. Wang, A unified glassy rheology for granular matter, arXiv:2604.14109.

[38] F. P. Bretherton, The motion of rigid particles in a shear flow at low Reynolds number, J. Fluid Mech. **14**, 284 (1962).

[39] E. DeGiuli, J. N. McElwaine, and M. Wyart, Phase diagram for inertial granular flows, Phys. Rev. E **94**, 012904 (2016).

[40] P. G. de Gennes and J. Prost, *The Physics of Liquid Crystals*, *International Series of Monographs on Physics*, 2nd ed. (Oxford University Press, Oxford, New York, 1995).

[41] T. A. Marschall, D. Van Hoesen, and S. Teitel, Shear-driven flow of athermal, frictionless, spherocylinder suspensions in two dimensions: Particle rotations and orientational ordering, Phys. Rev. E **101**, 032901 (2020).

[42] M. C. Marchetti, J. F. Joanny, S. Ramaswamy, T. B. Liverpool, J. Prost, M. Rao, and R. A. Simha, Hydrodynamics of soft active matter, Rev. Mod. Phys. **85**, 1143 (2013).

[43] D. Vescovi, B. Nadler, and D. Berzi, Simple generalization of kinetic theory for granular flows of nonspherical, oriented particles, Phys. Rev. Fluids **9**, L012301 (2024).

[44] D. Berzi, D. Vescovi, and B. Nadler, Shaking into order: Q-tensor/kinetic theory of vibrated non-spherical grains in a confined geometry, J. Fluid Mech. **1024**, A32 (2025).

[45] M. Trulsson, Directional shear jamming of frictionless ellipses, Phys. Rev. E **104**, 044614 (2021).

[46] A. Franceschini, E. Filippidi, E. Guazzelli, and D. J. Pine, Transverse alignment of fibers in a periodically sheared suspension: An absorbing phase transition with a slowly varying control parameter, Phys. Rev. Lett. **107**, 250603 (2011).

[47] J. Bilotto, M. Trulsson, and J.-F. Molinari, Orientation statistics of dense granular flow of elongated particles [Dataset], Zenodo, 2026, https://doi.org/10.5281/zenodo.23163286.

[48] J. Bilotto, Data_processing_orientations [Software], 2026, https://github.com/JBil8/Data_processing_orientations.